Received: 13 January 2024 | Revised: 21 June 2024 | Accepted: 2 July 2024

DOI: 10.1111/ocr.12835

RESEARCH ARTICLE

Orthodontics & Craniofacial Research WILEY

Sella turcica and facial bones: Morphological integration in the human fetal cranium

Natsuko Utsunomiya[1,2] | Motoki Katsube[1] | Yutaka Yamaguchi[2] | Masanori Kumakiri[1,2] | Naoki Morimoto[1] | Shigehito Yamada[2]

[1]Department of Plastic and Reconstructive Surgery, Graduate School of Medicine, Kyoto University, Kyoto, Japan

[2]Congenital Anomaly Research Center, Graduate School of Medicine, Kyoto University, Kyoto, Japan

Correspondence
Motoki Katsube, Department of Plastic and Reconstructive Surgery, Graduate School of Medicine, Kyoto University, Kyoto, Japan.
Email: katsube@kuhp.kyoto-u.ac.jp

Funding information
Japan Society for the Promotion of Science, Grant/Award Number: JP 23KJ1285, 21K16922, 21H01333 and 23H03209

Abstract

Objectives: The cranial base plays a significant role in facial growth, and closer analyses of the morphological relationship between these two regions are needed to understand the morphogenesis of the face. Here, we aimed to study morphological integration between the sella turcica (ST) and facial bones during the fetal period using geometric morphometrics.

Materials and Methods: Magnetic resonance images of 47 human fetuses in the Kyoto Collection, with crown-rump lengths of 29.8–225 mm, were included in this study. Anatomical homologous landmarks and semilandmarks were registered on the facial bones and the midsagittal contour of the ST, respectively. The shape variations in the craniofacial skeleton and the ST were statistically investigated by reducing dimensionality using principal component analysis (PCA). Subsequently, the morphological integration between the facial bones and ST was investigated using two-block partial least squares (2B-PLS) analysis.

Results: PCA showed that small specimens represented the concave facial profile, including the mandibular protrusion and maxillary retrusion. The 2B-PLS showed a strong integration (RV coefficient = 0.523, $r = .79$, $p < .01$) between the facial bones and ST. The curvature of the anterior wall of the ST was highly associated with immature facial morphology characterized by a concave profile.

Conclusion: The strong integration between the two regions suggested that the anterior ST may be associated with facial morphology. This result quantitatively confirms previous studies reporting ST deformities in facial anomalies and induces further research using postnatal subjects.

KEYWORDS
facial growth, fetal cranium, geometric morphometrics, morphological integration, sella turcica

1 | INTRODUCTION

The human face has unique characteristics, including a retruded and upright profile, converged eyes or a prominent nose, which is distinguishable from other animals. Much has been discussed regarding the mechanism of how facial morphology is determined; however, its elucidation remains challenging because facial development can be affected by the growth of various organs and interact with numerous factors, including genetic and environmental factors, such as tooth eruption and muscular activities.[1] Additionally, the human face has diversity in shape among populations or even within a population.[2] Previous studies[3,4] have indicated that shape variations in the facial skeleton of fetuses could be already observed in the second and third trimesters, which implies that facial shape could fluctuate and be modulated through the prenatal period.

The skull is divided into two subunits, the viscerocranium (facial bones) and the neurocranium, with the latter comprising the cranial base and vault. These structures have different embryological origins and follow different growth processes to develop their functions. According to the functional matrix theory by Moss,[5] the development of facial bones can be affected by functional matrices, including all soft tissues constructing the facial structure; facial bones develop in response to extrinsic factors. In contrast, the cranial base has an independent growth potential,[6] retaining intrinsic information of phenotypic importance.[1,7] Many studies have suggested that the cranial base plays significant roles in craniofacial growth, mainly explained by several synchondroses that remain as non-ossified zones in the cranial base from the prenatal to the postnatal period.[6,8–10] Previous morphometric analyses revealed correlations between the morphologies of the cranial base and the face, proposing the importance of the cranial base in facial orientation.[11–13] Geometric morphometric analyses by Bastir and Rosas[14] and Katsube et al.[15] in the fields of the human evolution and embryology, respectively, statistically revealed a morphological integration between the facial bones and cranial base. These two studies both suggested that the shape variation of the middle cranial fossa, especially the sphenoidal area, was involved in the midfacial projection; however, it raised the problem of elucidating what fine morphological variations in the middle cranial base can be related to the facial shape. In line with this, the sphenoidal area, which holds a significant potential of regulating the facial shape, seems a logical starting point for subsequent studies.

The sella turcica (ST) is a small recess in the body of the sphenoid that houses the pituitary gland and is often an important structure in morphometric studies of the craniofacial field. For instance, its center point, typically called the 'S' point, is one of the essential landmarks of lateral cephalograms in clinical practices. Such a focus on the ST has produced many reports describing abnormal ST shapes in patients with various craniofacial anomalies, which led researchers to realize that craniofacial anomalies are often accompanied by a shape deformation of the ST. Kjær[16] proposed the 'craniofacial patterning theory', which states that the ST can be divided into several different cranial fields according to fetal pathological condition: the frontonasal, maxillary, palatine, mandibular and cerebellar fields. She advocated that these areas of the ST have a potential for specific fetal pathology and that anomalies in a specific facial field often accompany a similar deformation at a specific location of the ST. This mapping of the ST region brought us to perceive the association between the ST shape and facial development or specific facial morphology; however, no quantitative analyses have supported this theory so far.

In light of these considerations, we speculated that a morphological relation between the face and ST could also exist in fetuses with morphological immaturity and fluctuation during development and that there might be specific patterns between the morphological traits of the face and ST. Therefore, this study aimed to analyse the morphological integration between the facial bones and ST during human fetal period using geometric morphometrics and contribute to understanding the shape variation of the ST in relation to normal facial development or congenital anomalies.

2 | MATERIALS AND METHODS

2.1 | Samples and data acquisition

The Kyoto Collection, stored at the Congenital Anomaly Research Center of Kyoto University, contains a large number of formalin-fixed human embryos and fetuses that have been obtained after artificial abortion since the 1960s, as per the Maternity Protection Law of Japan.[17,18] In this study, 47 fetuses with no obvious congenital anomalies in their appearances and no injury in the craniofacial region were selected from the Kyoto Collection. The sample information is shown in Table S1. The crown-rump length (CRL) of the samples ranged from 29.8 to 225 mm, and their gestational ages, estimated using Sahota's equation,[19] ranged from 9.9 to 20.6 weeks. In the fetal cranium, endochondral bones remain as cartilage in various degrees; as such, computed tomography (CT), which is usually used to study adult bones, does not reflect the actual morphology, especially when the subjects include a range of fetal ages. Therefore, in this study, magnetic resonance (MR) imaging was used for analyses instead of CT. MR imaging was performed using a 7T MR system (BioSpec 70/20 USR; Bruker BioSpin MRI GmbH, Ettlingen, Germany) and a 3T MR system (MAGNETOM Prisma; Siemens Healthcare, Erlangen, Germany).

2.2 | Landmark definition and registration

Landmarks were selected to capture the morphology of the face and cranial base. The landmarks on the face were digitized on the maxilla, zygoma, nasal bone, palate and mandible to reflect both the front and lateral morphology of the face. Landmarks on the cranial base were digitized on the anterior and middle cranial fossa. These landmarks were defined on anatomically homologous points according to previous studies,[14,15,20–22] and 75 three-dimensional landmarks were

registered on MR images using Checkpoint software (Stratovan, Davis, California) (Table 1 and Figure 1A). To assess the measurement error of the landmarks, ten of all specimens were randomly selected, and the landmark sets were registered by two different raters. The analysis was performed by Procrustes ANOVA using 'gm.measurement.error' function in the *geomorph* package. Intra-class correlation between raters was very high ($r=0.998$), suggesting that the measurement error was negligible relative to the biological variation of interest. All the coordinates of these landmarks were imported into 3D Slicer software.[23] Then, to represent the shape of the ST, semilandmarks, which were automatically set at even intervals between two or more landmarks, were registered in the midsagittal plane of the MR images using 3D Slicer software. The anterior and posterior terminals of the ST were defined as the most convex midline point of the tuberculum sellae (#4) and the tip of the dorsum sellae (#5), respectively. Thirteen semilandmarks (#76–88) were placed between the two points (#4 and #5), comprising a total of 15 points, to represent the midsagittal contour of the ST floor (Table 1 and Figure 1B,C). Semilandmarks are not biologically homologous points themselves, and a sliding process is needed to optimize their positions with respect to the average shape.[24] The sliding of the semilandmarks was performed three times using the 'slider3d' function in the *Morpho* package.

2.3 | Multivariate shape analyses

Multivariate shape analyses based on geometric morphometrics were performed using the acquired landmarks and semilandmarks. Pre-processing of the coordinates was performed before the shape analyses to exclude extra information other than the shape information (Figure 2). First, generalized Procrustes analysis (GPA), including a scaling, translation and rotation of all coordinates, was performed on the full sets of original coordinates.[25] Our subjects included fetuses at various gestational weeks, and the centroid size calculated through GPA was set as the size variable which indicates fetal growth. Second, axial rotation of the mandibular coordinates was performed to correct the mouth-opening degree among specimens as previously described,[21] as formalin-fixed fetal samples have various mouth-opening positions. The corrected coordinates acquired through these processes were used for the subsequent shape analyses.

To investigate the morphological relation between the facial bones and ST, we analysed the following: (1) shape variation of the facial bones and cranial base, (2) shape variation of the ST in the midsagittal plane and (3) morphological integration between the facial bones and ST. For the first step, principal component analysis (PCA), a dimensionality reduction method that summarizes morphological variations among specimens, was performed on all sets of coordinates. This step was performed to understand the global trend of shape variation in the facial bones and cranial base among all samples. Next, PCA on the 15 semilandmarks of the ST was performed to study the shape variation of the ST in the midsagittal plane. To investigate the shape allometry of the ST, the correlation between the centroid size and principal component (PC) scores was tested using the ordinary least squares approach. Finally, the morphological integration between the facial bones and ST was investigated using two-block partial least squares (2B-PLS) analysis, a statistical approach used to assess the morphological relationship between phenotypic traits by investigating the covariation pattern between sets of landmarks.[26] The landmarks were divided into two blocks (Table 1): Block 1 (the facial bones) consisting of 49 landmarks of the midface and mandible and Block 2 (the ST) consisting of 15 semilandmarks of the ST; 2B-PLS was performed between these two blocks.

The axial rotation of the mandibular coordinates was carried out using MATLAB 9.0.1 software (Mathworks, Natick, MA, USA). All analyses except for this were carried out using software R version 4.0.1 (R Core Team, 2020), including the *Morpho*[27] and *geomorph*[28] packages.

2.4 | 3D visualization of the results

The results of the shape analyses were visualized as 3D models using a step-by-step method (Figure S1). First, the 3D model of the craniofacial bone of the reference specimen was created via manual segmentation on the MR images using the 3D Slicer segmentation module. This reference model was warped by reflecting the mean shape coordinates of all the samples to create the mean shape model. Next, the target model (result model) was created using this mean shape model as follows: the target coordinates of the objective shapes to be visualized were first estimated using the PC or PLS scores, then the mean shape model was warped by projecting the target coordinates to create the target model. Finally, a color-contrasted model was generated to visualize the local shape differences between the target models reflecting the 2B-PLS results. These visualization processes were performed using R software. The color-contrasted model was created using the 'localmeshdiff' function in the *Arothron* R package.[29]

2.5 | Ethical considerations

This study was conducted with the approval of the ethics committee of the affiliation. Verbal informed consent was obtained from the parents of all participants.

3 | RESULTS

3.1 | Shape variation of the facial bones and cranial base

PC1 and PC2 explained 43.53% and 10.02% of the total variance, respectively, whereas PC3 explained only 6.18%. When we observed the 3D models reflecting each PC, the shape variation of the PC1 axis was large and apparent, while that of PC2 was much

TABLE 1 Definitions of the landmarks and semilandmarks.

No.	Landmark	Detailed information	Region	Block 1 or 2
1	Foramen caecum	Most anterior inferior point of the anterior midline cranial base	Cranial base	–
2	Posterior cribriform	Midline point at the posterior end of the cribriform plate	Cranial base	–
3	Sphenoidale	Most superior and posterior midline point on the tuberculum sellae	Cranial base	–
4	Tuberculum sellae	Most convex midline point of the tuberculum sellae	Cranial base	2
5	Dorsum sellae	Most superior and posterior midline point on the dorsum sellae	Cranial base	2
6	Basion	Lowest point on the anterior margin of the foramen magnum	Cranial base	–
7, 8	Anterior lateral cribriform	Most anterior and lateral points of the cribriform plate	Cranial base	–
9, 10	Posterior lateral cribriform	Most posterior and lateral points of the cribriform plate	Cranial base	–
11, 12	Anterior cranial base (antero-lateral)	Most anterior and lateral points of the anterior cranial base	Cranial base	–
13, 14	Anterior cranial base (lateral)	Most lateral points of the anterior cranial base	Cranial base	–
15, 16	Posterior frontal	Point at which the posterior border of the anterior fossa fuses with the endocranial lateral wall	Cranial base	–
17, 18	Anterior clinoid process	Most superior, posterior and medial points of the anterior clinoid process	Cranial base	–
19, 20	Optic canal	Most posterior medial points of the margin of the optic canal	Cranial base	–
21, 22	Foramen rotundum	Most posterior medial points of the margin of the foramen rotundum	Cranial base	–
23, 24	Internal acoustic meatus	Most posterior lateral points of the margin of the internal acoustic meatus	Cranial base	–
25	Nasion	Most concave point on the midline between the nasal bone and frontal bone	Midface	1
26	Rhinion	Midline point at the inferior end of the internasal suture	Midface	1
27	Nasal septum (anterior)	Most anterior point of the nasal septum	Midface	1
28	Anterior nasal spine	Most superior anterior midline point of the anterior nasal spine	Midface	1
29	Subspinale	Deepest midline point in the curved bony outline from the base to the alveolar process of the maxilla	Midface	1
30	Incisive fossa	Most inferior anterior point of the margin of the incisive fossa	Midface	1
31	Nasal septum (inferior posterior)	Most inferior posterior point of the nasal septum	Midface	1
32, 33	Nasolacrimal duct	Most superior medial points of the margin of the nasolacrimal duct	Midface	1
34, 35	Alare	Most inferior lateral points on the margin of the nasal aperture	Midface	1
36, 37	Infraorbital foramen	Most inferior anterior points of the margin of the infraorbital foramen	Midface	1
38, 39	Orbital rim (lateral)	Most anterior lateral points of the inferior orbital rim	Midface	1

(Continues)

TABLE 1 (Continued)

No.	Landmark	Detailed information	Region	Block 1 or 2
40, 41	Jugale	Point in the depth of notch between the temporal and frontal processes of the zygomatic bone	Midface	1
42, 43	Premaxillary maxillary suture	Most inferior lateral points of the premaxillary maxillary suture	Midface	1
44, 45	Root of the zygomatic process	Most inferior, anterior and medial points of the zygomatic process	Midface	1
46, 47	Greater palatine foramen	Most inferior, posterior and medial margins of the greater palatine foramen	Midface	1
48, 49	Posterior alveolar	Most posterior points of the alveolar process on the inferior surface of the maxilla	Midface	1
50, 51	Hamulus of the medial pterygoid plate	Most inferior points of the Hamulus of the medial pterygoid plate	Cranial base	–
52	Superior mandibular symphysis	Most superior anterior point of the mandibular symphysis	Mandible	1
53	Gnathion	Most inferior anterior point of the mandibular symphysis	Mandible	1
54, 55	Mental tubercle	Most inferior anterior points of the mental tubercle	Mandible	1
56, 57	Mandibular foramen	Most inferior posterior points of the mental foramen	Mandible	1
58, 59	Gonion	Most inferior posterior points of the masseter muscle attachment	Mandible	1
60, 61	Condyle	Most posterior lateral points of the condylar process	Mandible	1
62, 63	Coronion	Most superior posterior points of the coronoid process	Mandible	1
64, 65	Mandibular notch	Points in the depth of the mandibular notch	Mandible	1
66, 67	Central incisor	Most inferior points of the tooth bud of the central incisor	Mandible	1
68, 69	Lateral incisor	Most inferior points of the tooth bud of the lateral incisor	Mandible	1
70, 71	Canine	Most inferior points of the tooth bud of the canine	Mandible	1
72, 73	First molar	Most inferior points of the tooth bud of the first molar	Mandible	1
74, 75	Second molar	Most inferior points of the tooth bud of the second molar	Mandible	1
76–88	Midsagittal shape of the ST	Semilandmarks between No. 4 and 5 set along the contour of ST in the midsagittal plane	Cranial base	2

Abbreviation: ST, sella turcica.

smaller. Therefore, we considered PC1 was dominant, PC2 was subdominant, and PC3 and the rest were minor components in explaining the shape. Figure 3A shows a scatter plot of the PC1 and PC2 scores, and the plotted points were painted in gradient colors corresponding to the value of the CRL. Specimens with a small CRL had negative scores on the PC1 axis, while those with a large CRL had positive scores, suggesting that PC1 was associated with shape allometry. Figure 3B shows the extreme shapes along the PC1 axis. The extreme negative shape of the PC1 axis (small CRL) showed a concave profile, which was characterized by a protrusion of the mandible, retrusion of the maxilla, anteroposterior shortness of the nasal septum, and a flat and small zygoma. The other facial features observed in PC1 negative were a narrow mandible, wide maxilla and piriform aperture, and wide interorbital distance. The midline region of the cranial base was large and wide relative to whole basicranial areas: the sphenoid

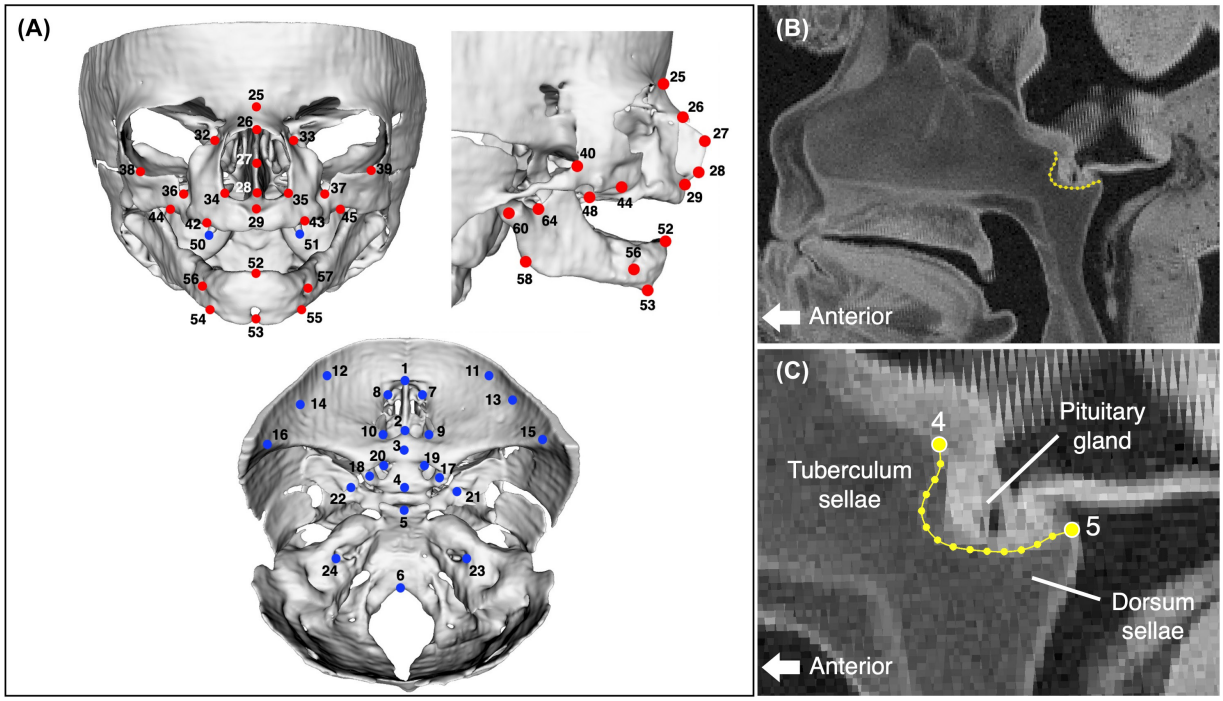

FIGURE 1 Landmarks and semilandmarks in this study. (A) Anatomical landmarks are shown on the reference 3D model. Landmarks of the midface and the mandible are indicated in red, and those of the cranial base are in blue. Some landmarks are not visible in these 3D models. See Table 1 for detailed information. (B and C) Midsagittal plane of the magnetic resonance image. Thirteen semilandmarks are registered at even intervals between two landmarks of the sella turcica (ST) (#4 and #5) to compose a total of 15 points representing the midsagittal contour of the ST (yellow).

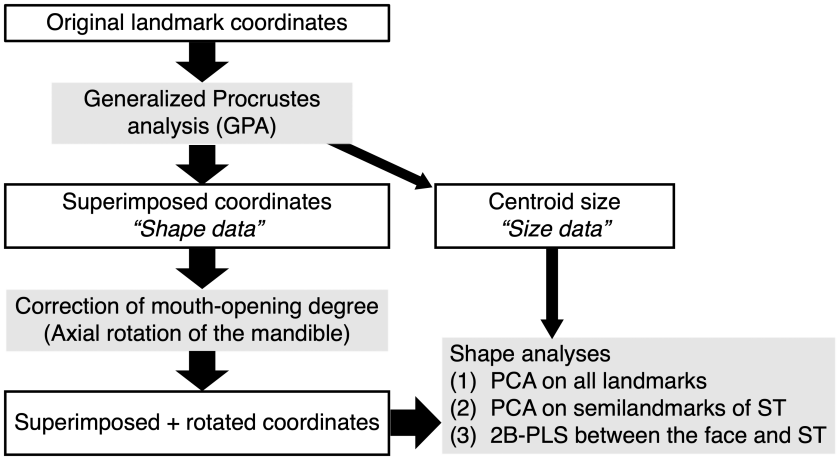

FIGURE 2 Pre-processing of the landmark coordinates. First, GPA was performed on all sets of original coordinates of landmarks and semilandmarks to the best superimposition. The centroid size was extracted as the size information by this process and used as the size variable in this study. Next, the axial rotation of the mandibular landmarks was performed using MATLAB software to unify the mouth-opening degree among samples. 2B-PLS, two-block partial least squares; GPA, generalized Procrustes analysis; PCA, principal component analysis; ST, sella turcica.

body was wide, the greater and lesser wings inclined to the horizontal and anterior directions, respectively, and the cribriform plate was wide and short in the anteroposterior direction. The extreme positive shape of the PC1 axis (large CRL) showed an opposite pattern to the PC1 negative: the mandible was set back, the midface protruded anteriorly, the zygoma was enlarged and the anterior and middle cranial base were relatively narrow. The ST was roughly visible in the 3D models; however, a detailed shape could not be assessed. Figure 3B also shows the models of extreme shapes along the PC2 axis. PC2 was associated with the

anteroposterior position of the mandible and maxilla, the width of the maxilla and the entire face, and the width of the anterior and middle area of the cranial base. According to the scatter plot shown in Figure 3A, the PC2 axis had little relation with the CRL in small specimens and indicated an allometric pattern in large specimens. This suggested that there was a large variation in shape features until a certain developmental stage; after that, it tended to converge in more limited features.

3.2 | Shape variation of the ST in the midsagittal plane

The first two components accounted for >70% (PC1 and PC2 at 42.02% and 29.58%, respectively), while PC3 accounted for only 13.20%. Owing to the rapid decrease in the contribution rate after PC3, we consider that the shape variation of the midsagittal ST was summarized by PC1 and PC2. A scatter plot of the PC1 and PC2

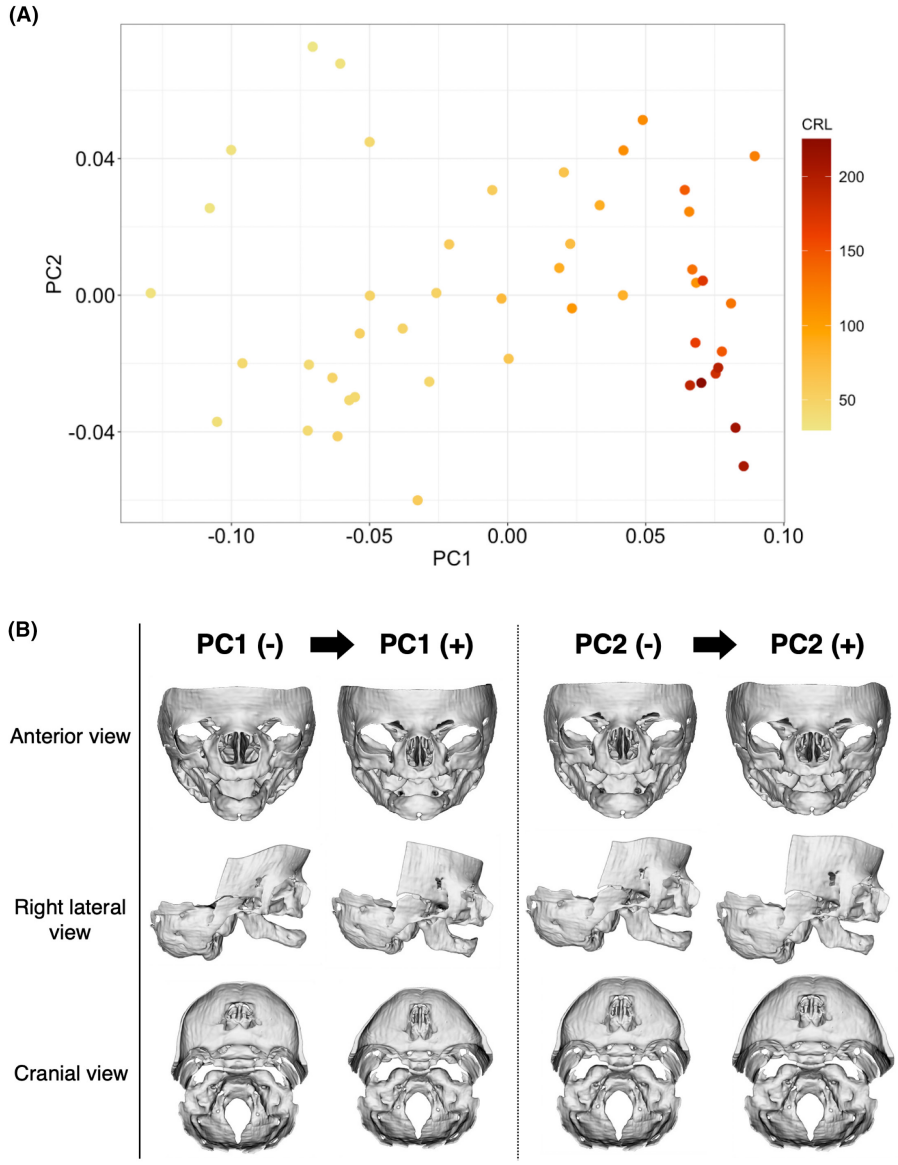

FIGURE 3 The result of PCA on the facial bones and cranial base. (A) Scatter plot of the PC scores of the first two axes (PC1 and PC2). The plotted points are painted with gradient colors corresponding to the value of the CRL. PC1 explained 43.53% of the total variance, while PC2 explained 10.02%. In the PC1 axis, specimens with a small CRL were distributed in the PC1 negative and those with a large CRL in the PC1 positive, indicating that PC1 explained the shape variation along development (shape allometry). (B) Extreme shapes of the PC1 (left) and PC2 (right) axes are shown. The extreme negative shape of PC1, indicating specimens with a small CRL, is characterized by a protruded mandible, a retruded and wide maxilla, and a small and flat zygoma. Shape variations of the cranial base along the PC1 axis are mainly observed in the width of the midline area; in PC1 negative, the cranial base has a wide and short cribriform plate and a wide sphenoidal area. However, the shape variation of the ST cannot be observed precisely in these models. In the PC2 axis, shape variations are associated with the anteroposterior position of the mandible and maxilla, the width of the maxilla and the entire face, and the width of the anterior and middle areas of the cranial base. CRL, crown-rump length; PC, principal component; PCA, principal component analysis; ST, sella turcica.

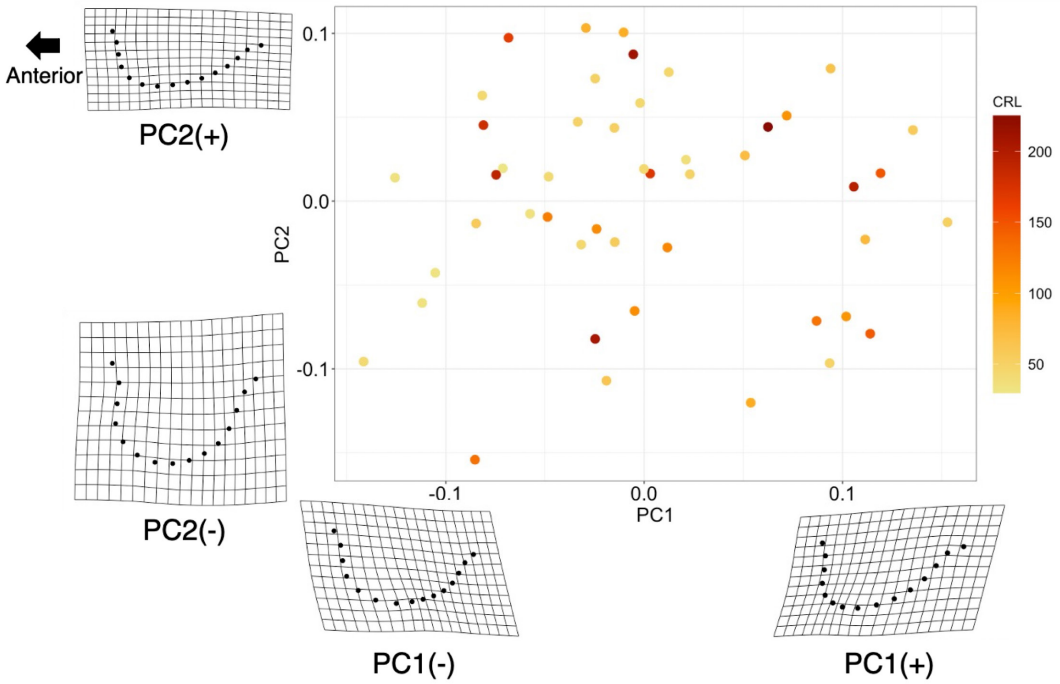

FIGURE 4 The result of PCA on the midsagittal shape of the ST. The scatter plot of PC1 and PC2 scores and the TPS grids of the extreme shapes explained by the PC1 and PC2 axes are shown. The plotted points are painted in gradient colors corresponding to the value of the CRL. The distribution of CRL is irregular either in PC1 or PC2 axes. The left side of each TPS grid shows the anterior of the ST, and the right side is the posterior. PC1 is related to the obliqueness of the entire shape, the width of the ST floor, and the gradual curve of the anterior wall. In the PC1 positive shape, in comparison with the negative, the deepest point of the floor is in the anterior and the floor is narrow. PC2 is related to the depth of the floor and the curve of the anterior wall. These shape variations of the ST had little relation with allometry because the PC scores of PC1 and PC2 had no correlation with the centroid size (see Figure S2). PCA, principal component analysis; ST, sella turcica; TPS, thin-plate spline.

scores is shown in Figure 4, with thin-plate spline (TPS) deformation grids visualizing extreme shapes along the first and second PC axes. The PC1 axis was associated with an obliqueness of the entire shape, the width of the ST floor, and the curve of the anterior wall. In the extreme positive shape of the PC1 axis, the deepest point of the floor moved to the anterior, the floor was narrow, and the anterior wall showed a gradual curve. The PC2 axis was associated with the depth of the ST. The extreme positive shape of the PC2 axis was characterized by a flat ST, while the extreme negative shape was characterized by a deep floor with a gradual inverse S-shaped curve of the anterior wall. Ordinary least squares regression showed no significant correlation between PC1 and centroid size ($R^2 < .01$, $p = .19$) or between PC2 and centroid size ($R^2 < .01$, $p = .89$) (Figure S2), suggesting that the shape variation of the ST had little relation with allometry.

3.3 | Morphological integration between the facial bones and ST

The first PLS axis explained 84.64% of the total covariance between the two landmark blocks, while the second explained only 13.93%; the remaining axes had contributions smaller than 1%. The RV coefficient of PLS1 was 0.523 ($r = .79$, $p < .01$), indicating a strong integration between the facial bones and ST. The PLS scores of each block for the first pair of PLS1 are plotted in Figure 5A. The extreme shape of each block along the PLS1 axis is visualized individually in Figure 5B: 3D models for the facial bones (Block 1) and 2D TPS grids for the ST (Block 2). The color-contrasted models on the upper right portion of Figure 5B visualize the local shape differences between the PLS1 positive and negative shapes of the facial bones. The extreme negative shape of the facial bones (Block 1) along the PLS1 axis showed that the mandible protruded anteriorly, with a length extension around the mental foramen. The maxilla was wide and short anteroposteriorly, and the zygoma was flat and small. Additionally, the interorbital distance and piriform aperture were wide, the nasal bone was wide and relatively short, and the coronoid process of the mandible was small. The extreme negative shape of the ST (Block 2) along the PLS1 axis was characterized by a gradual inverse S-shaped curve of the anterior wall. The extreme positive shape of the facial bones showed the opposite pattern of the PLS1 negative, characterized by a setback of the mandible and protrusion of the maxilla. The ST had a straight and short anterior wall in the PLS1 positive. Whereas the anterior wall showed the shape change between the PLS1 negative and positive, the posterior wall showed few shape differences. In summary, this analysis statistically showed a strong integration between the facial bones and the midsagittal contour of the ST, highlighting the morphological relation between

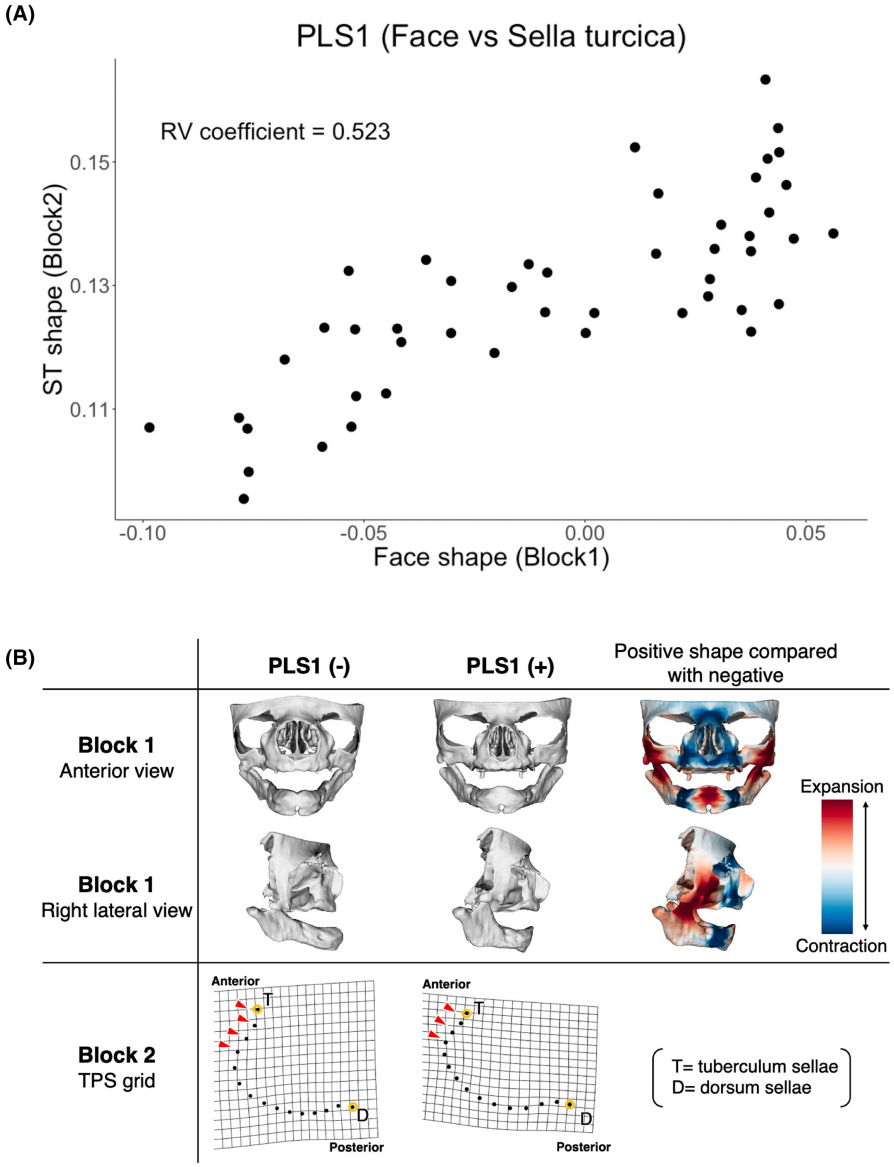

FIGURE 5 Result of the 2B-PLS analysis between the facial bones and ST. (A) PLS scores of each block for the first pairs of the PLS1 axis (84.64% of the total covariance) are plotted. The RV coefficient between the two blocks was 0.523 ($r = .79$, $p < .01$), indicating a strong integration between the facial bones and ST. (B) Shape variations of Block 1 (the facial bones) and Block 2 (the ST), explained by the extreme negative or positive scores along the PLS1 axis, are shown. Upper and middle rows (Block 1): The extreme negative shape of the PLS1 axis shows a concave profile characterized by a protrusion of the mandible, a retrusion of the maxilla, and a small and flat zygoma. It shares these traits with specimens with small CRLs shown in the first PCA. The PLS1 positive shape is opposite that of the negative. The 3D models with a color map show local differences between the positive and negative shapes, reflecting the shape differences on the positive model. Blue colors show local contraction, while red colors show local enlargement. Lower row (Block 2): The extreme negative shape of the ST is characterized by a gradual inverse S-shaped curve in the anterior wall, whereas the extreme positive shape shows a straight and short anterior wall and a relatively shallow floor (red arrowheads). In contrast, few shape changes were observed in the posterior wall. These grids were warped with a factor of 1.5 to emphasize the shape differences. 2B-PLS, two-block partial least squares; PCA, principal component analysis; ST, sella turcica.

the face and the anterior wall of the ST. Furthermore, the features of the concave face observed in the PLS1 negative were shared with those of the small CRL specimens in the first PCA on all landmarks. Accordingly, this result suggested that the anterior wall curvature of the ST was related to immature facial morphology.

4 | DISCUSSION

Previous studies reported that anomalies in the midfacial region are often accompanied by abnormal shape of the anterior wall of the ST. For example, Down's syndrome has typical facial features

characterized as midfacial hypoplasia and malocclusion class III mainly derived from maxillary retrusion.[30] Russel and Kjær[31] reported that the ST in patients with Down's syndrome had a higher rate of obliqueness and depression in the anterior wall than in normal individuals. Korayem and Alkofide[32] reported that the size of the ST in patients with Down's syndrome was abnormal, with a higher rate of abnormal variations such as an oblique anterior wall or the bridging of the ST. Various deformities of the anterior ST have also been identified in patients with cleft lip and palate,[33] skeletal malocclusion[34] and other craniofacial anomalies related to genetic syndromes.[35] The morphological relation between the facial anomalies and ST is summarized in Kjær's craniofacial patterning theory,[16,36] which suggests that the anterior part of the ST has pathological potential in the frontonasal and maxillary fields. These studies suggest that the anterior region of the ST probably interacts with the facial morphology; however, no studies so far have performed quantitative analyses to confirm them. Our current study aimed to quantitatively investigate the morphological relation between the facial bones and ST during the fetal period. Our 2B-PLS analysis showed a strong integration between the facial bones and ST. The PLS1 axis explained that a curved anterior wall of the ST was related to the immature facial morphology, characterized by a protruded mandible, a retruded maxilla, and a small zygoma.

In contrast, the posterior wall of the ST showed little variation in the 2B-PLS analysis. We believe this is not a product of chance; it may have resulted from the difference in embryonic origins between the anterior and posterior parts of the cranial base, which are derived from the neural crest cells and paraxial mesoderm, respectively[37,38]; the anterior part shares its origin with the facial bones. A recent study on embryonic tissue origins using transgenic mice elucidated the neural crest-mesoderm border in mice in detail.[38] The difference in behavior between the anterior and posterior ST shown in our study could remind us of the importance of the border of tissue origins to understand craniofacial morphogenesis.

A possible clinical application of this study could be to analyse postnatal subjects. The distinctive feature of ST shape in a specific craniofacial anomaly could be applicable to screening for the anomaly. Moreover, a previous study suggested that some shape variations in the ST were also observed in the normal population[22]; hence, we speculated that shape variations of the anterior ST in the normal population may be related to individual diversities in midfacial morphology. In light of this, studying healthy subjects of various ages may be helpful to better understand the basic facial development or the derivation of individuality in human facial shape. Furthermore, previous studies have indicated that there are morphological differences in the ST shape between racial groups and the sexes in the postnatal population,[39] which may also support morphological relationships between the ST and facial shape. No comparison between racial or sex groups was performed in this study owing to a unified race (Japanese) and a small sample size. Comparative analyses would provide further insight into the mechanism of facial morphogenesis.

There are several limitations in this study. First, the range of fetal stages in this study was limited owing to the size of the MR imaging coil, which is considered a confounding factor that could have artificially separated actual growth and influenced the results. Second, landmark registration of the ST was limited to two-dimensional due to a lack of appropriate 3D anatomical points on the fetal ST. However, we consider that such 2D analysis using the midsagittal plane could be beneficial for future reference because, in clinical practices, the ST shape is generally observed using lateral cephalograms and 2D examinations are more available and accessible than 3D examinations. Third, we could not study the growth of the pituitary gland using our samples because of organ contractions caused by formalin fixation. As the pituitary gland develops prior to the chondrogenesis of the ST, it is hypothesized to affect the shape of the ST[16]; however, even in vivo studies using mice might not address this problem because mice do not have an obvious deep depression of the ST around the pituitary gland as that in humans.[38,40] Further consideration using postnatal human samples will be needed to yield any findings about the influence of the function and development of the pituitary gland.

Despite these limitations, the facial bones and the anterior wall of the ST showed a strong morphological integration during the fetal period. Further investigation using postnatal samples, including normal and anomalous populations, will provide more insights into the relationship between the face and ST. According to our study, even a minute structure in the cranial base can potentially interact with drastic morphological changes in the face. We believe that further quantitative studies on the fine morphology of the cranial base will contribute to elucidation of the human-specific facial development and the mechanisms of congenital craniofacial anomalies.

5 | CONCLUSIONS

In the present study, a high RV coefficient between the facial bones and ST of normal human fetuses was shown through 2B-PLS analysis, suggesting a strong morphological integration between the immature morphology of the facial bones and a curved anterior wall of the ST. This study is the first to statistically investigate the morphological relation between the face and the fine structure in the cranial base, quantitatively supporting previous findings that shape deformations of the anterior ST are often observed in midfacial anomalies. Further studies with postnatal samples, including both normal and abnormal populations, would support our suggestions and help better understand human craniofacial development.

AUTHOR CONTRIBUTIONS

N.U. designed the study, acquired the data, performed the analyses, prepared all of the figures and wrote the manuscript. M.K. acquired imaging data and contributed to performing the analyses. Y.Y. acquired imaging data. N.U., M.K., M.K. and S.Y. contributed to data interpretation. M.K., S.Y. and N.M. participated in the critical

revision of the manuscript. All authors read and approved the final manuscript.

ACKNOWLEDGEMENTS

We thank Ms. Chigako Uwabe of the Congenital Anomaly Research Center at Kyoto University for technical assistance in handling human fetal samples. This work was supported by the Grant-in-Aid for JSPS Fellows (Grant Number JP 23KJ1285) and the Japan Society for the Promotion of Science KAKENHI (Grant Numbers 21K16922, 21H01333 and 23H03209). We would like to thank Editage (www.editage.jp) for English language editing.

CONFLICT OF INTEREST STATEMENT

The authors have no conflicts of interest directly related to the content of this article.

DATA AVAILABILITY STATEMENT

The data that support the findings of this study are available on request from the corresponding author. The data are not publicly available due to privacy or ethical restrictions.

ETHICAL APPROVAL

This study was approved by the Kyoto University Graduate School and Faculty of Medicine Ethics Committee (approval no. R0316 and R0347). Verbal informed consent was obtained from the parents of all participants.

REFERENCES

1. Herring SW. Formation of the vertebrate face: epigenetic and functional influences. *Am Zool*. 1993;33(4):472-483. doi:10.1093/icb/33.4.472
2. Kanavakis G, Silvola AS, Halazonetis D, Lahdesmaki R, Pirttiniemi P. Profile shape variation and sexual dimorphism amongst middle-aged northern Europeans. *Eur J Orthod*. 2022;44(1):30-36. doi:10.1093/ejo/cjab004
3. Mandarim-de-Lacerda CA, Alves MU. Growth of the cranial bones in human fetuses (2nd and 3rd trimesters). *Surg Radiol Anat*. 1992;14(2):125-129. doi:10.1007/BF01794887
4. Michael Plavcan J, German RZ. Quantitative evaluation of craniofacial growth in the third trimester human. *Cleft Palate Craniofac J*. 1995;32(5):394-404. doi:10.1597/1545-1569_1995_032_0394_qeocgi_2.3.co_2
5. Moss ML. A theoretical analysis of the functional matrix. *Acta Biotheor*. 1968;18(1):195-202. doi:10.1007/BF01556727
6. Scott JH. The cranial base. *Phys Anthropol*. 1958;16(3):319-348. doi:10.1002/ajpa.1330160305
7. Lieberman DE, Hallgrímsson B, Liu W, Parsons TE, Jamniczky HA. Spatial packing, cranial base angulation, and craniofacial shape variation in the mammalian skull: testing a new model using mice. *J Anat*. 2008;212(6):720-735. doi:10.1111/j.1469-7580.2008.00900.x
8. Jeffery N, Spoor F. Ossification and midline shape changes of the human fetal cranial base. *Am J Phys Anthropol*. 2004;123(1):78-90. doi:10.1002/ajpa.10292
9. Opperman LA, Gakunga PT, Carlson DS. Genetic factors influencing morphogenesis and growth of sutures and synchondroses in the craniofacial complex. *Semin Orthod*. 2005;11(4):199-208. doi:10.1053/j.sodo.2005.07.004
10. Rosenberg P, Arlis HR, Haworth RD, Heier L, Hoffman L, LaTrenta G. The role of the cranial base in facial growth: experimental craniofacial synostosis in the rabbit. *Plast Reconstr Surg*. 1997;99(4):1396-1407.
11. Bastir M, Rosas A, Stringer C, et al. Effects of brain and facial size on basicranial form in human and primate evolution. *J Hum Evol*. 2010;58(5):424-431. doi:10.1016/j.jhevol.2010.03.001
12. Lieberman DE, Ross CF, Ravosa MJ. The primate cranial base: ontogeny, function, and integration. *Am J Phys Anthropol*. 2000;113:117-169. doi:10.1002/1096-8644(2000)43:31+<117::aid-ajpa5>3.3.co;2–9
13. Bastir M, Rosas A. Correlated variation between the lateral basicranium and the face: a geometric morphometric study in different human groups. *Arch Oral Biol*. 2006;51(9):814-824. doi:10.1016/j.archoralbio.2006.03.009
14. Bastir M, Rosas A. Cranial base topology and basic trends in the facial evolution of homo. *J Hum Evol*. 2016;91:26-35. doi:10.1016/j.jhevol.2015.11.001
15. Katsube M, Yamada S, Yamaguchi Y, et al. Critical growth processes for the midfacial morphogenesis in the early prenatal period. *Cleft Palate Craniofac J*. 2019;56(8):1026-1037. doi:10.1177/1055665619827189
16. Kjær I. Sella turcica morphology and the pituitary gland – a new contribution to craniofacial diagnostics based on histology and neuroradiology. *Eur J Orthod*. 2015;37(1):28-36. doi:10.1093/ejo/cjs091
17. Yamada S, Nakano S, Makishima H, Motoki T. Novel imaging modalities for human embryology and applications in education. *Anat Rec*. 2018;301(6):1004-1011. doi:10.1002/ar.23785
18. Yamada S, Nagai M, Hagiwara M. The 40th anniversary of the congenital anomaly research center, Kyoto University graduate School of Medicine. *Anat Rec*. 2018;301(6):947-950. doi:10.1002/ar.23786
19. Sahota DS, Leung TY, Leung TN, Chan OK, Lau TK. Fetal crown-rump length and estimation of gestational age in an ethnic Chinese population. *Ultrasound Obstet Gynecol*. 2009;33(2):157-160. doi:10.1002/uog.6252
20. Neaux D, Guy F, Gilissen E, Coudyzer W, Ducrocq S. Covariation between midline cranial base, lateral basicranium, and face in modern humans and chimpanzees: a 3D geometric morphometric analysis. *Anat Rec*. 2013;296(4):568-579. doi:10.1002/ar.22654
21. Katsube M, Yamada S, Utsunomiya N, et al. A 3D analysis of growth trajectory and integration during early human prenatal facial growth. *Sci Rep*. 2021;11(1):6867. doi:10.1038/s41598-021-85543-5
22. Axelsson S, Storhaug K, Kjær I. Post-natal size and morphology of the sella turcica. Longitudinal cephalometric standards for Norwegians between 6 and 21 years of age. *Eur J Orthod*. 2004;26(6):597-604. doi:10.1093/ejo/26.6.597
23. Fedorov A, Beichel R, Kalpathy-Cramer J, et al. 3D slicer as an image computing platform for the quantitative imaging network. *Magn Reson Imaging*. 2012;30(9):1323-1341. doi:10.1016/j.mri.2012.05.001
24. Gunz P, Mitteroecker P. Semilandmarks: a method for quantifying curves and surfaces. *Hystrix It J Mamm*. 2013;24(1):103-109. doi:10.4404/hystrix-24.1-6292
25. Rohlf FJ, Slice D. Extensions of the Procrustes method for the optimal superimposition of landmarks. *Syst Zool*. 1990;39(1):40-59. doi:10.2307/2992207
26. Klingenberg CP. Evolution and development of shape: integrating quantitative approaches. *Nat Rev Genet*. 2010;11(9):623-635. doi:10.1038/nrg2829
27. Schlager S. Chapter 9 – Morpho and Rvcg – shape analysis in R: R-packages for geometric Morphometrics, shape analysis and surface manipulations. In: Zheng G, Li S, Székely G, eds. *Statistical Shape and Deformation Analysis*. Academic Press; 2017:217-256.

28. Adams DC, Collyer M, Kaliontzopoulou A, Sherratt E. Geomorph: Software for geometric morphometric analyses. R package version 4.0.7. Available at https://cran.r-project.org/package=geomorph
29. Antonio P, Costantino B, Silvia C, et al. Arothron: an R package for geometric morphometric methods and virtual anthropology applications. *Am J Phys Anthropol*. 2021;176(1):144-151. doi:10.1002/ajpa.24340
30. Suri S, Tompson BD, Cornfoot L. Cranial base, maxillary and mandibular morphology in down syndrome. *Angle Orthod*. 2010;80(5):861-869. doi:10.2319/111709-650.1
31. Russell BG, Kjær I. Postnatal structure of the sella turcica in down syndrome. *Am J Med Genet*. 1999;87(2):183-188. doi:10.1002/(sici)1096-8628(19991119)87:2<183::aid-ajmg11>3.0.co;2-a
32. Korayem M, Alkofide E. Size and shape of the sella turcica in subjects with down syndrome. *Orthod Craniofac Res*. 2015;18(1):43-50. doi:10.1111/ocr.12059
33. Nielsen BW, Mølsted K, Kjær I. Maxillary and sella turcica morphology in newbornswith cleft lip and palate. *Cleft Palate Craniofac J*. 2005;42(6):610-617. doi:10.1597/04-104r.1
34. Valizadeh S, Shahbeig S, Mohseni S, Azimi F, Bakhshandeh H. Correlation of shape and size of sella turcica with the type of facial skeletal class in an Iranian group. *Iran J Radiol*. 2015;12(3):e16059. doi:10.5812/iranjradiol.12(3)2015.16059
35. Roomaney IA, Chetty M. Sella turcica morphology in patients with genetic syndromes: a systematic review. *Orthod Craniofac Res*. 2021;24(2):194-205. doi:10.1111/ocr.12426
36. Kjær I. Orthodontics and foetal pathology: a personal view on craniofacial patterning. *Eur J Orthod*. 2010;32(2):140-147. doi:10.1093/ejo/cjp059
37. Noden DM, Trainor PA. Relations and interactions between cranial mesoderm and neural crest populations. *J Anat*. 2005;207(5):575-601. doi:10.1111/j.1469-7580.2005.00473.x
38. McBratney-Owen B, Iseki S, Bamforth SD, Olsen BR, Morriss-Kay GM. Development and tissue origins of the mammalian cranial base. *Dev Biol*. 2008;322(1):121-132. doi:10.1016/j.ydbio.2008.07.016
39. Muhammed FK, Abdullah AO, Liu Y. Morphology, incidence of bridging, dimensions of sella turcica, and cephalometric standards in three different racial groups. *J Craniofac Surg*. 2019;30(7):2076-2081. doi:10.1097/scs.0000000000005964
40. Kathleen Pitirri M, Kawasaki K, Richtsmeier JT. It takes two: building the vertebrate skull from chondrocranium and dermatocranium. *Vertebr Zool*. 2020;70(4):587-600. doi:10.26049/VZ70-4-2020-04

SUPPORTING INFORMATION

Additional supporting information can be found online in the Supporting Information section at the end of this article.

How to cite this article: Utsunomiya N, Katsube M, Yamaguchi Y, Kumakiri M, Morimoto N, Yamada S. Sella turcica and facial bones: Morphological integration in the human fetal cranium. *Orthod Craniofac Res*. 2024;27:938-949. doi:10.1111/ocr.12835